Inorganic Chemistry

Article

pubs.acs.org/IC

Catalytic Water Oxidation by a Molecular Ruthenium Complex: Unexpected Generation of a Single-Site Water Oxidation Catalyst

Wangchuk Rabten,[†] Markus D. Kärkäs,*[,†] Torbjörn Åkermark,[†] Hong Chen,[‡,§] Rong-Zhen Liao,[∥] Fredrik Tinnis,[†] Junliang Sun,[‡,⊥] Per E. M. Siegbahn,[†] Pher G. Andersson,*[,†] and Björn Åkermark*[,†]

[†]Arrhenius Laboratory, Department of Organic Chemistry, and [‡]Berzelii Centre EXSELENT on Porous Materials, Department of Materials and Environmental Chemistry, Stockholm University, SE-106 91 Stockholm, Sweden

[§]Faculty of Material Science and Chemistry, China University of Geosciences, 430074, Wuhan, China

[∥]Key Laboratory for Large-Format Battery Materials and System, Ministry of Education, School of Chemistry and Chemical Engineering, Huazhong University of Science and Technology, 430074, Wuhan, China

[⊥]College of Chemistry and Molecular Engineering, Peking University, 100871, Beijing, China

Supporting Information

ABSTRACT: The increasing energy demand calls for the development of sustainable energy conversion processes. Here, the splitting of H_2O to O_2 and H_2, or related fuels, constitutes an excellent example of solar-to-fuel conversion schemes. The critical component in such schemes has proven to be the catalyst responsible for mediating the four-electron oxidation of H_2O to O_2. Herein, we report on the unexpected formation of a single-site Ru complex from a ligand envisioned to accommodate two metal centers. Surprising N−N bond cleavage of the designed dinuclear ligand during metal complexation resulted in a single-site Ru complex carrying a carboxylate−amide motif. This ligand lowered the redox potential of the Ru complex sufficiently to permit H_2O oxidation to be carried out by the mild one-electron oxidant $[Ru(bpy)_3]^{3+}$ (bpy = 2,2′-bipyridine). The work thus highlights that strongly electron-donating ligands are important elements in the design of novel, efficient H_2O oxidation catalysts.

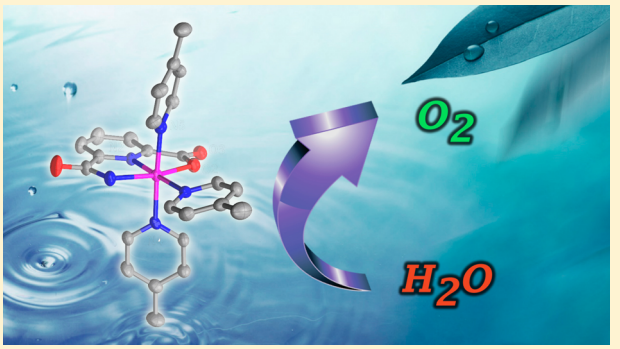

INTRODUCTION

In attempts to store solar energy as chemical energy, such as H_2, artificial photosynthetic schemes are attractive. However, the design of efficient catalysts for the oxidation of H_2O to yield O_2, electrons, and protons (eq 1), where the two latter can combine to give H_2, has proved challenging.[1−3]

$$2H_2O \rightarrow 4H^+ + 4e^- + O_2 \quad (1)$$

Nature performs this complicated task by utilizing a Mn_4O_5Ca cluster that efficiently carries out the four-electron oxidation of H_2O to O_2.[4] The lack of robust and efficient artificial water oxidation catalysts (WOCs) thus hampers the design of H_2O splitting devices and has therefore been a hot topic for researchers to pursue.[5] Artificial molecular WOCs based on Mn,[6−10] Fe,[11−14] Co,[15−17] and Cu[18−20] have been constructed but Ir[21−23] and, especially, Ru[24−35] seem to be superior and eventuate in robust molecular catalysts. The incorporation of negatively charged functional entities into the ligand scaffolds of WOCs has proved to be a promising strategy for the controlled design of molecular Ru catalysts.[36−39] The reason is that the negatively charged ligands stabilize the metal center(s) at high redox states via extensive electron donation.[40,41] This stabilizing effect further reflects in the significantly reduced redox potentials compared to WOCs bearing neutral polypyridyl ligands.

Incorporation of negatively charged amide[24] and carboxylate[37] groups has previously proved to give viable candidates for inclusion into ligand architectures of WOCs. It was therefore envisioned that a combination of these motifs in a single unit could create a suitable ligand environment. The tailored ligand **1**, which could be accessed through straightforward synthesis from readily available building blocks (Figure 1) containing the hydrazide unit, seemed to be a promising candidate for generation of a dinuclear Ru complex.

However, the single-site Ru complex **3** was unexpectedly generated via N−N bond cleavage of ligand **1** (Figure 2). The produced Ru complex **3** containing the tridentate 6-carbamoylpicolinic acid ligand **4** (H_3L) was also synthesized independently and characterized and was found to possess appealing catalytic properties which allowed H_2O oxidation to be driven by $[Ru(bpy)_3]^{3+}$ (bpy = 2,2′-bipyridine). Electrochemical measurements confirmed that the complex exhibited lower redox potentials than Ru WOCs bearing neutral ligand

Received: November 21, 2014

DOI: 10.1021/ic502755c
Inorg. Chem. XXXX, XXX, XXX−XXX

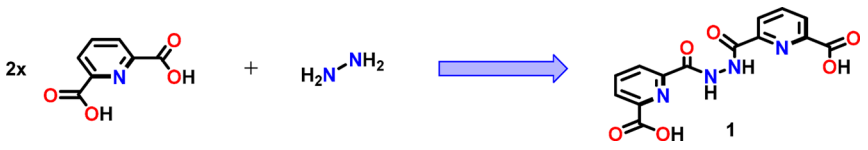

Figure 1. Envisioned assembly of ligand **1**.

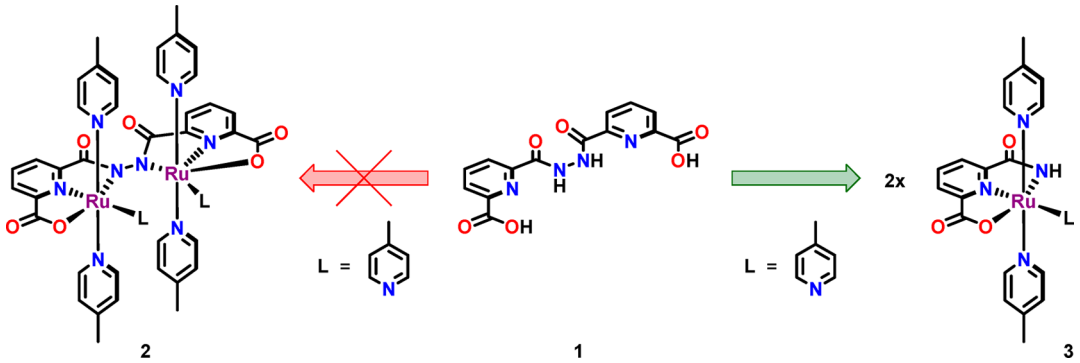

Figure 2. Generation of the single-site Ru complex **3** from ligand **1** via N−N bond cleavage.

Scheme 1. Synthesis of Ligand 1

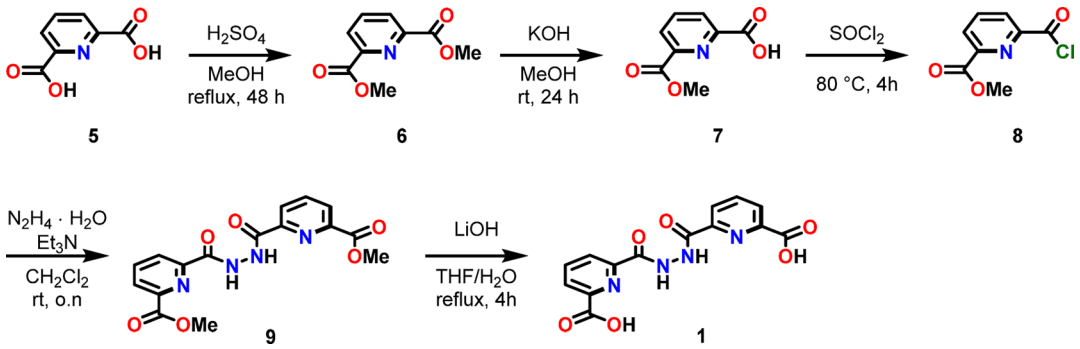

Scheme 2. Synthesis of Ligand 4

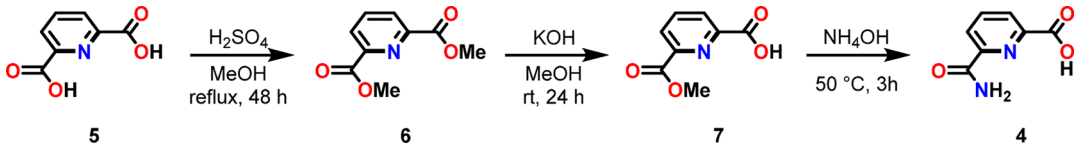

scaffolds. The introduction of amide functional groups to WOCs could thus be a general strategy for constructing more efficient catalysts with reduced onset potentials. In addition, this work highlights that the inclusion of sensitive functional motifs into ligand scaffolds could result in conversion to unexpected structures. Care, therefore, has to be taken when crafting ligand scaffolds as they might be subjected to further transformation into unmapped metal complexes that are the actual WOCs.

RESULTS AND DISCUSSION

Synthesis, Characterization and Crystal Structure of Ru Complex 3. Ligand **1** was synthesized according to Scheme 1, starting from the readily available pyridine-2,6-dicarboxylic acid (**5**). Refluxing compound **5** in MeOH in the presence of H_2SO_4 resulted in the dimethyl pyridine-2,6-dicarboxylate ester **6**. Selective hydrolysis of one of the ester moieties gave the pyridine-2,6-dicarboxylate monomethyl ester **7**, which was subsequently transformed into acyl chloride **8**. Treatment of compound **8** with hydrazine hydrate ($N_2H_4{\cdot}H_2O$) converted **8** into the dimethyl ester **9**. Finally, hydrolysis with LiOH gave the dinuclear ligand **1** as a white solid.

Attempts to obtain a dinuclear Ru complex based on ligand **1** by refluxing the ligand with $Ru(DMSO)_4Cl_2$ as the metal precursor only resulted in reductive cleavage of the N−N bond to yield a single-site Ru complex (**3**). The structure of the single-site complex was characterized as $[Ru(HL)(pic)_3]^+$ by ^1H NMR spectroscopy (after reduction to Ru^{II}), mass spectrometry, UV−vis spectroscopy, and X-ray crystallography (vide infra). Independent synthesis of ligand **4**, according to Scheme 2, and Ru complex **3** further confirmed the structure of the single-site Ru complex **3**.

Suitable single crystals for X-ray diffraction of Ru complex **3** were obtained by cooling a solution of complex **3** in MeCN/EtOAc (1:9), and the structure is presented in Figure 3. The resolved crystal structure revealed that the Ru^{III} is located in a slightly distorted $[RuN_5O]$ octahedral configuration. In the equatorial plane, three positions are occupied by two nitrogen

DOI: 10.1021/ic502755c
Inorg. Chem. XXXX, XXX, XXX−XXX

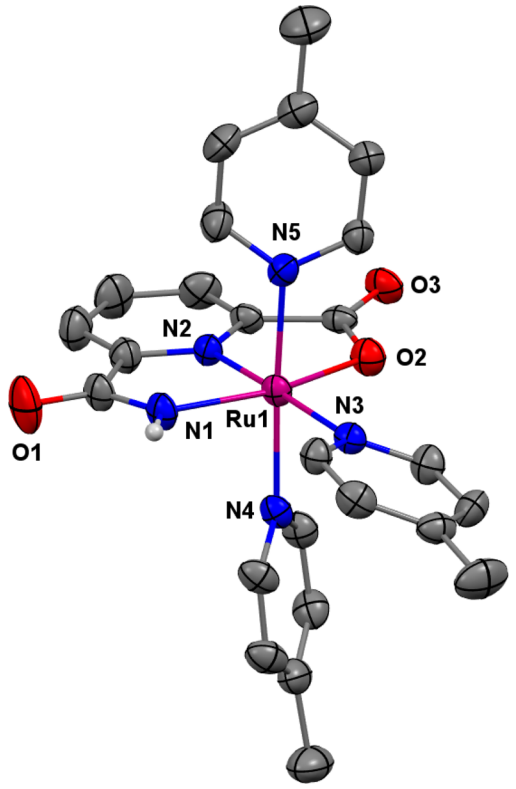

Figure 3. X-ray crystal structure of the single-site Ru complex **3**. Hydrogen atoms (except the N−H) have been omitted for clarity.

and one oxygen atoms from the tridentate 6-carbamoylpicolinic acid ligand **4** and one position is contributed by the nitrogen atom from a 4-picoline ligand. The two axial positions are both occupied by 4-picoline ligands.

Compared to the crystal structure of $[Ru^{II}(pdc)(pic)_3]$ (**10**; where H_2pdc = 2,6-pyridinedicarboxylic acid), a previously reported WOC,[42] the open angle in Ru complex **3** [N(1)−Ru(1)−O(2)] is close to the one found for this complex. However, the corresponding Ru1−O2(carboxyl) and Ru−N(pic) bonds of complex **3** are considerably shorter (cf. Table 1 and Figure 4). Quantum chemical calculations have previously shown that a proton acceptor near the active site of Ru WOCs favors proton-coupled electron-transfer (PCET) processes. These PCET events are fundamental for accessing high-valent Ru species since they avoid the formation of high-energy intermediates via concerted proton−electron move-

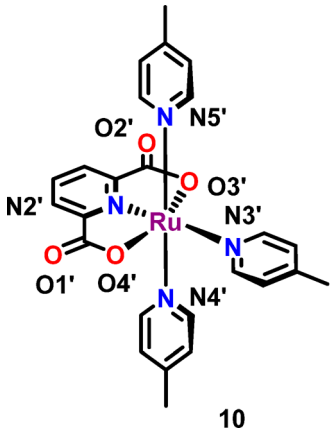

10

Bond lengths (Å)

Ru-N2'	1.947
Ru-N3'	2.078
Ru-N4'	2.068
Ru-N5'	2.092
Ru-O3'	2.119
Ru-O4'	2.146

Figure 4. Structure of the previously reported $[Ru^{II}(pdc)(pic)_3]$ complex **10** (where H_2pdc = 2,6-pyridinedicarboxylic acid) with selected bond lengths.

ment.[43] A similar hydrogen-bonding effect is also expected in aqueous solutions for Ru complex **3**, which houses two possible proton handles, the amide and carboxyl units.

O_2 Evolution Activity. The performance of Ru complex **3** to mediate H_2O oxidation was evaluated at neutral conditions (aqueous phosphate buffer; 0.1 M, pH 7.2) with the mild one-electron chemical oxidant $[Ru(bpy)_3]^{3+}$. The amount of produced O_2 was monitored in real time by mass spectrometry. Upon the addition of an aqueous solution containing complex **3** to the solid oxidant, O_2 evolution could immediately be detected (Figure 5). The low O_2 evolution yields, i.e., conversion yields from oxidant to O_2, in Table 2 are due to decomposition of the $[Ru(bpy)_3]^{3+}$ oxidant in neutral aqueous solutions and contribute to unproductive reaction pathways. In the absence of any catalyst, the $[Ru(bpy)_3]^{3+}$ oxidant thus spontaneously decomposes without generation of O_2.

The initial rate of O_2 evolution was shown to be proportional to the initial concentration of complex **3** (Figure 6 and Supporting Information). Assuming pseudo-first-order kinetics, the initial rate of O_2 evolution can be approximated by eq 2. The measured rate constant k_{O2} (0.58) can subsequently be converted to yield the turnover frequency (TOF), which equals 1.16 s^{-1}.[44] The calculated TOF of Ru complex **3**, 1.16 s^{-1}, is approximately 1 order in magnitude greater than the TOFs (using Ce^{IV} as the chemical oxidant) of the previously developed $[Ru(tpy)(bpy)(OH_2)]^{2+}$-type complexes (tpy = 2,2′:6′,2″-terpyridine), which are based on neutral polypyr-

Table 1. Selected Bond Lengths (Å) and Angles (deg) for Ru Complex 3

Bond Lengths (Å)			
Ru(1)−N(2)	1.958(3)	Ru(1)−N(4)	2.087(3)
Ru(1)−N(1)	2.024(3)	Ru(1)−N(5)	2.095(3)
Ru(1)−O(2)	2.043(3)	Ru(1)−N(3)	2.108(3)
Bond Angles (deg)			
N(2)−Ru(1)−N(1)	79.60(12)	N(4)−Ru(1)−N(5)	176.77(12)
N(2)−Ru(1)−O(2)	80.44(12)	N(2)−Ru(1)−N(3)	178.07(13)
N(1)−Ru(1)−O(2)	160.00(12)	N(1)−Ru(1)−N(3)	100.19(12)
N(2)−Ru(1)−N(4)	92.37(12)	O(2)−Ru(1)−N(3)	99.73(11)
N(1)−Ru(1)−N(4)	88.54(13)	N(4)−Ru(1)−N(3)	85.70(12)
O(2)−Ru(1)−N(4)	91.10(12)	N(5)−Ru(1)−N(3)	91.41(12)
N(2)−Ru(1)−N(5)	90.52(12)	O(2)−Ru(1)−N(5)	87.95(11)
N(1)−Ru(1)−N(5)	93.40(13)		

DOI: 10.1021/ic502755c
Inorg. Chem. XXXX, XXX, XXX−XXX

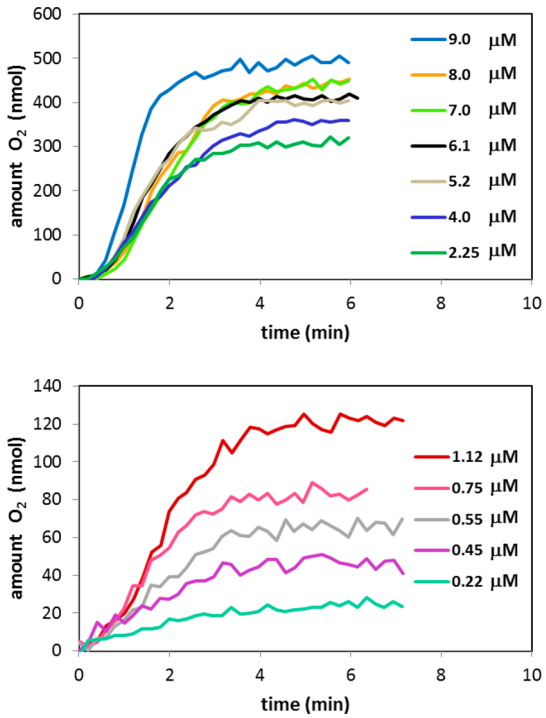

Figure 5. Plots of O_2 evolution vs time at various concentrations of Ru complex **3**. Reaction conditions: experiments were carried out by addition of an aqueous phosphate buffer solution (0.1 M, pH 7.2, 0.50 mL) containing catalyst **3** in varying concentrations to the oxidant $[Ru(bpy)_3](PF_6)_3$ (3.6 mg, 3.6 μmol).

Table 2. Summary of the Catalytic Data for Ru Complex 3[a]

catalyst concn (μM)	TON (nmol O_2/nmol cat.)[b]	yield of O_2 (4 × nmol O_2/nmol oxidant) (%)
9.0	110	55
8.0	114	51
7.0	134	52
6.1	140	47
5.2	155	45
4.0	185	41
2.25	280	35
1.12	220	14
0.75	235	9.8
0.55	250	7.8
0.45	225	5.6
0.22	230	2.8

[a]Reaction conditions: An aqueous phosphate buffer solution (0.1 M, pH 7.2, 0.50 mL) containing Ru complex **3** was added to the oxidant $[Ru(bpy)_3](PF_6)_3$ (3.6 mg, 3.6 μmol). [b]Turnover numbers (TONs) were calculated from moles of produced O_2/moles of catalyst.

idyl-type ligand scaffolds. The TOF value of Ru complex **3** (1.16 s^{-1}) is also higher than the TOF value reported for the related $[Ru(pdc)(pic)_3]$ complex (0.23 s^{-1})[47] but is significantly lower than the TOF values reported for the $[Ru(bda)(pic)_2]$-type complexes[33] (H_2bda = 2,2′-bipyridine-6,6′-dicarboxylic acid) which, however, use Ce^{IV} as the chemical oxidant.

$$\text{initial rate } O_2 \text{ evolution} = k_{O2}[\mathbf{3}] \quad (2)$$

Ligand Exchange. The four-electron oxidation of H_2O requires the accumulation of multiple redox equivalents at the catalytic entity. This can be regulated by the simultaneous transfer of electrons and protons, enabling PCET,[45,46] which

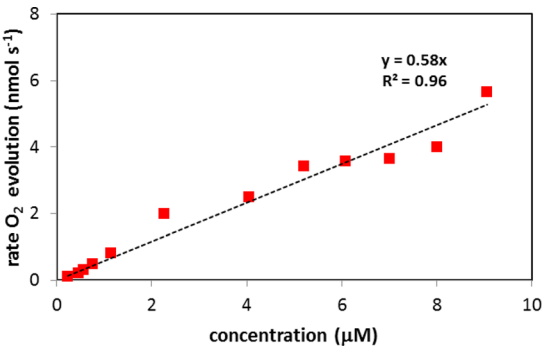

Figure 6. Initial rate of O_2 evolution plotted as a function of the concentration of Ru complex **3**. From the obtained k_{O2} (0.58), the turnover frequency (TOF) can be calculated. This gives a TOF of ~1.16 s^{-1} (for further information see Supporting Information).

significantly reduces the redox potentials of the metal complex and hence lowers the catalytic onset potential at which H_2O is being oxidized. In order to generate the catalytically active intermediate, Ru complex **3** has to undergo picoline−H_2O ligand exchange where one of the picoline ligands is replaced by a solvent aqua ligand. Initial experiments in trying to detect the important Ru−aqua species made use of ^1H NMR. However, the ^1H NMR spectrum of the Ru complex **3** did not show any apparent peaks arising from the paramagnetic nature of the Ru^{III} center. The Ru^{III} center was therefore reduced to Ru^{II} by addition of ascorbic acid, a reductant, to a solution of complex **3** in CD_3OD. The acquired ^1H NMR spectrum now revealed clear and sharp peaks. Analysis of the derived spectrum showed integrals corresponding to the structure $[Ru^{II}(HL)(pic)_3]$ (Supporting Information Figures S7−S9). It was further demonstrated that "free 4-picoline" was absent in the reduced sample (Supporting Information Figure S8). On the basis of these observations, it is clear that substitution of the picoline ligand by an aqua or solvent molecule does not occur to any appreciable extent at the Ru^{II} state. Electrospray ionization mass spectrometry (ESI-MS) was subsequently used to study the ligand dissociation at the Ru^{III} state. Analysis of an aqueous solution of Ru complex **3** resulted in the appearance of a peak at m/z 470.0544, corresponding to $[Ru^{III}(HL)(pic)_2(OH_2)]^+$ (Figure 7). This observation indicates that picoline−aqua ligand exchange does occur for Ru complex **3** at the Ru^{III} state, enabling PCET and easy access to higher redox states, which ultimately brings about the facile conversion of H_2O into O_2. Quantum chemical calculations showed that the picoline−H_2O ligand displacement is favored at the equatorial position by 2.9 kcal mol^{-1}.

Electrochemical Properties. In order to get a deeper understanding of the catalytic properties of Ru complex **3**, electrochemical measurements were carried out. It is important to realize that the involvement of picoline−aqua ligand exchange may complicate the interpretation of the electrochemical behavior of Ru complex **3**. The electrochemistry of Ru complex **3** was initially assessed by cyclic voltammetry (CV) under neutral conditions, in an aqueous phosphate buffer solution (0.1 M, pH 7.2) and is depicted in Figure 8. A distinct rise in the current was observed at E = 1.17 and is ascribed to the onset of a catalytic current for H_2O oxidation. In order to obtain the potentials for the different redox couples, differential pulse voltammetry (DPV) was subsequently measured at neutral pH. DPV revealed three peaks at 0.35, 0.72, and 0.92 V vs NHE, which were assigned to the Ru^{III}/Ru^{II}, Ru^{IV}/Ru^{III},

DOI: 10.1021/ic502755c
Inorg. Chem. XXXX, XXX, XXX−XXX

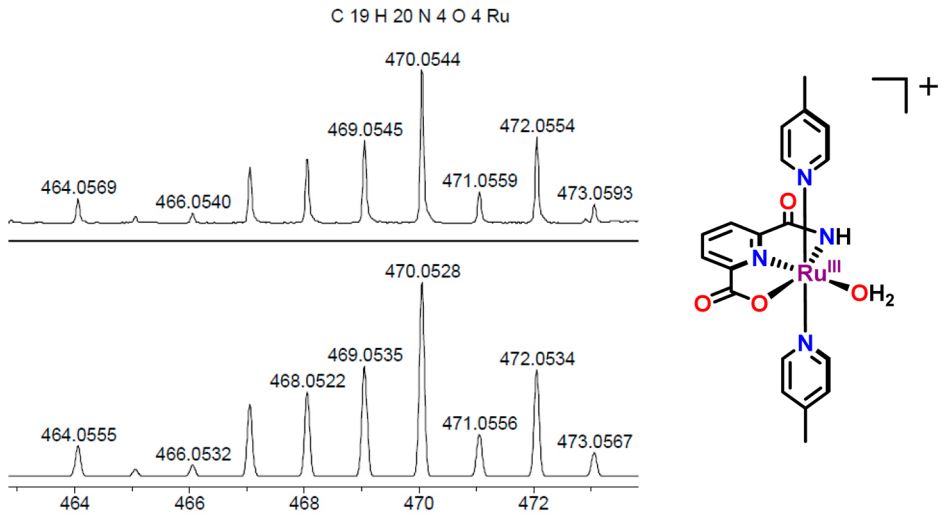

Figure 7. (Upper) Experimental high-resolution mass spectrum of the corresponding Ru^{III}–aqua species of Ru complex **3** ($[Ru^{III}(HL)(pic)_2(OH_2)]^+$) in positive mode and (lower) the simulated spectrum. pic = 4-picoline.

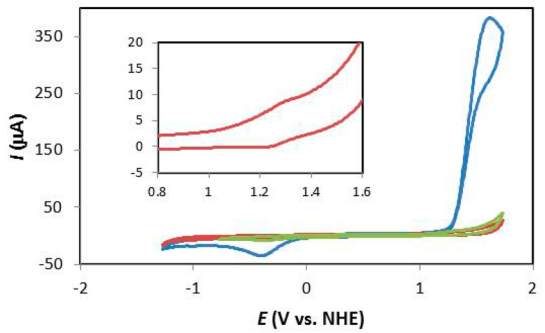

Figure 8. Cyclic voltammograms of Ru complex **3** (blue), $[Ru(bpy)_3]Cl_2$ (red) in an aqueous phosphate buffer solution (0.1 M, pH 7.2) together with pristine phosphate buffer (green). Inset: enlarged voltammogram of $[Ru(bpy)_3]Cl_2$ in the range $0.80 < E < 1.60$ V.

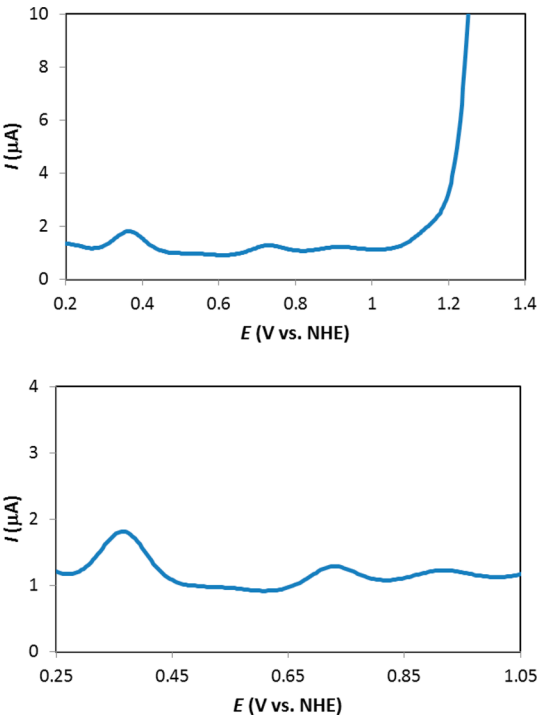

Figure 9. (Upper) Differential pulse voltammogram of Ru complex **3** at pH 7.2. (Lower) Enhanced view of the differential pulse voltammogram of Ru complex **3** at pH 7.2 in the range $0.25 < E < 1.05$ V. Conditions: voltammograms were recorded in aqueous phosphate buffer solutions (0.1 M, pH 7.2) containing Ru complex **3** (93 μM) with a scan rate of 0.1 V s^{-1}, using the $[Ru(bpy)_3]^{3+}/[Ru(bpy)_3]^{2+}$ couple as a standard ($E_{1/2}$ = 1.26 V vs NHE).

and Ru^V/Ru^{IV} redox couples, respectively (Figure 9). Table 3 summarizes the electrochemical results at pH 7.2.

The obtained redox potentials can be compared to the potentials for the previously reported, and structurally related, single-site $[Ru(pdc)(pic)_3]$ complex **10**, which bears two carboxylate moieties instead of having the carboxylate–amide motif as in Ru complex **3**. In an aqueous phosphate buffer solution (pH 7.0) containing 10% acetonitrile, at a scan rate of 100 mV s^{-1}, the $[Ru^{II}(pdc)(pic)_3]$ complex displayed three irreversible peaks at ~0.46, ~0.84, and ~1.05 V vs NHE.[42] Although the authors did not speculate on the individual redox events, in a subsequent paper the Ru^{IV}/Ru^{III} couple was calculated to occur at a potential of 0.78 V vs NHE at pH 7.0.[47] The catalytic onset potential for the $[Ru(pdc)(pic)_3]$ complex was found to occur at 1.26 V vs NHE at pH 7.2.[42] When comparing the redox potentials for the Ru complex **3** and the related $[Ru(pdc)(pic)_3]$ complex **10** at neutral conditions, it is clear that the amide motif in complex **3** is a better electron donor and hence reduces the individual redox couples and the catalytic onset potential of Ru complex **3** (see Table 3). This highlights that incorporation of amide units into the ligand frameworks of WOCs could be a general strategy for lowering the onset potential for H_2O oxidation.

Quantum Chemical Insight. In order to further confirm the different redox events occurring at pH 7.2, quantum chemical calculations were carried out at the B3LYP* level (see the Experimental Section for detailed information). We started off by calculating the redox potentials for the various Ru–picoline species (Figure 10). Interestingly, it was found that the amide motif could potentially coordinate either via the nitrogen or the oxygen atom, which results in the two Ru^{II} isomers $\mathbf{3}_{Ru^{II}O-pic}$ and $\mathbf{3}_{Ru^{II}N-pic}$, respectively, where the N-coordinated isomer ($\mathbf{3}_{Ru^{II}N-pic}$) was found to be 3.2 kcal mol^{-1} higher in energy. The redox events are thus expected to start with the

DOI: 10.1021/ic502755c
Inorg. Chem. XXXX, XXX, XXX–XXX

Table 3. Summary of the Electrochemical Data for Single-Site Ru Complex 3 and for the Related [Ru(pdc)(pic)$_3$] Complex

	$E_{1/2}$ (V vs NHE)			
	Ru complex **3**		[Ru(pdc)(pic)$_3$]	
redox couple	exptl[a]	calcd[b]	exptl[c]	calcd[d]
Ru^{III}/Ru^{II}	0.35	0.36	0.46	0.60
Ru^{IV}/Ru^{III}	0.72	0.76	0.84	0.78
Ru^{V}/Ru^{IV}	0.92	0.84	1.05	1.38
Ru^{VI}/Ru^{V}	[e]	1.30		

[a]Electrochemical measurements were performed in an aqueous phosphate buffer solution (0.1 M, pH 7.2). All potentials were obtained from DPV and are reported vs normal hydrogen electrode (NHE). Conditions: scan rate 0.1 V s^{-1}, glassy carbon disk as working electrode, a platinum spiral as counter electrode, and a saturated calomel electrode (SCE) as reference electrode. Potentials were converted to NHE by using the $[Ru(bpy)_3]^{3+}/[Ru(bpy)_3]^{2+}$ couple as a standard ($E_{1/2}$ = 1.26 V vs NHE). [b]Redox potentials were calculated at the B3LYP* level. [c]Electrochemical measurements were performed in an aqueous phosphate buffer solution (0.05 M, pH 7.0) containing 10% acetonitrile, at a scan rate of 0.1 V s^{-1} (see ref 42). [d]Redox potentials were calculated at the M06//B3LYP level (see ref 47). [e]The Ru^{VI}/Ru^{V} redox couple could not be observed, most likely due to its high reactivity.

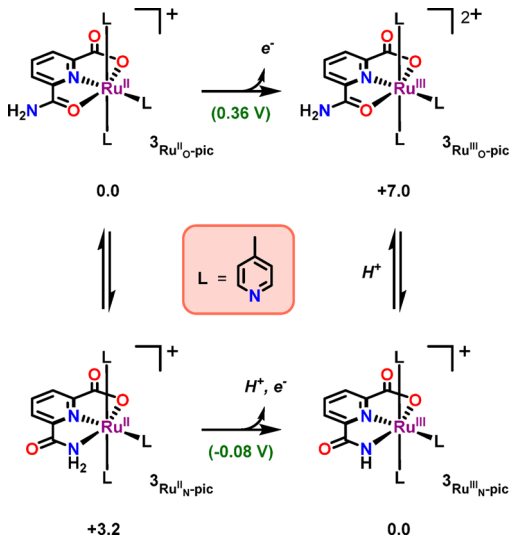

Figure 10. Overview of the various Ru–picoline intermediates at pH 7.2 with the formal redox states highlighted. Calculated redox potentials are shown in parentheses and are in volts vs normal hydrogen electrode (NHE), and the relative energies are given in kcal mol^{-1}.

Ru^{II}–picoline complex $\mathbf{3}_{Ru^{II}O-pic}$, which is oxidized to the corresponding Ru^{III} complex $\mathbf{3}_{Ru^{III}O-pic}$ at a potential of 0.36 V vs NHE (Figure 10), in accordance with the experimentally observed redox potential (0.35 V). This redox transition was found to be non-proton-coupled, even though the Ru^{II} complex possess a dissociable proton at the amide moiety, and originates from the strong electron-donating nature of the carboxylate–amide motif. The $\mathbf{3}_{Ru^{III}O-pic}$ species is then expected to undergo an O → N isomerization with a subsequent deprotonation to yield $\mathbf{3}_{Ru^{III}N-pic}$ (**3**), which is the complex that is isolated. The N-coordinated species $\mathbf{3}_{Ru^{III}N-pic}$ (**3**) was calculated to be 7.0 kcal mol^{-1} lower in energy than the O-coordinated species $\mathbf{3}_{Ru^{III}O-pic}$. The reduction of $\mathbf{3}_{Ru^{III}N-pic}$ to $\mathbf{3}_{Ru^{II}N-pic}$ was associated with a potential of −0.08 V and is in good agreement with our experimental measurement, in which the oxidation and reduction were found to be irreversible. At the Ru^{III} state, picoline–aqua ligand exchange is expected to take place, as observed experimentally, and generates the corresponding Ru^{III}–aqua complex.

The different Ru–aqua/hydroxo/oxo species for Ru complex **3** are depicted in Figure 11 together with their respective redox potentials. Picoline–aqua ligand exchange is thus expected to generate the Ru^{III}–aqua complex $\mathbf{3}_{Ru^{III}N}$ ($[Ru^{III}(HL)(pic)_2(OH)]$), where the related $\mathbf{3}_{Ru^{III}O}$ species was calculated to be 3.6 kcal mol^{-1} higher in energy. The optimized structures of the two species $\mathbf{3}_{Ru^{III}N}$ and $\mathbf{3}_{Ru^{III}O}$ are presented in Figure 12. As is shown in Figure 9, the following redox transition, Ru^{IV}/Ru^{III}, results in the formation of $\mathbf{3}_{Ru^{IV}N}$ ($[Ru^{IV}(HL)(pic)_2(O)]$) and was calculated to occur at a potential of 0.76 V, which is close to the experimentally observed potential of 0.72 V. The subsequent Ru^{V}/Ru^{IV} process is non-proton-coupled and was calculated to occur at 0.84 V, and yields $\mathbf{3}_{Ru^{V}N}$ ($[Ru^{V}(HL)(pic)_2(O)]^+$). The isomeric complex, $\mathbf{3}_{Ru^{V}O}$, was found to lie 10.8 kcal mol^{-1} higher in energy. The Ru^{VI}/Ru^{V} redox potential was also calculated and was associated with a potential of 1.30 V. The low redox potential associated with the Ru^{VI}/Ru^{V} transition suggests that the Ru^{V} species ($\mathbf{3}_{Ru^{V}N}$) is not responsible for triggering O–O bond formation. Most likely a further oxidation (not observed) to generate a species of higher valency is needed to bring about O–O bond formation. It should also be noted that the Ru^{III}/Ru^{II} transition for $\mathbf{3}_{Ru^{III}N}/\mathbf{3}_{Ru^{II}N}$ and $\mathbf{3}_{Ru^{III}O}/\mathbf{3}_{Ru^{II}O}$ were calculated to take place at low redox potentials, −0.22 and 0.04 V, respectively. These potentials differ significantly from the experimentally observed potential, which suggests that the Ru^{II}–aqua complex is not present in large quantities in solution at the Ru^{II} state. An overview of the various redox processes that are presumed to occur at neutral conditions, leading to O_2 liberation is presented in Scheme 3.

CONCLUSIONS

Herein we report on the unexpected cleavage of ligand **1**, resulting in the formation of the single-site Ru complex **3** bearing carboxylate and amide moieties. Complex **3** was also independently synthesized and characterized, in order to confirm the structure. The crystal structure of complex **3** revealed that the Ru center is in the Ru^{III} state because of the strong electron-donating ability of the 6-carbamoylpicolinic acid ligand **4**. This strong donor ability allowed chemical H_2O oxidation to be carried out with the mild one-electron oxidant $[Ru(bpy)_3]^{3+}$. Compared to the single-site Ru complex **3**, WOCs based on neutral nitrogen containing heterocyclic ligands are generally not compatible with the mild $[Ru(bpy)_3]^{3+}$ oxidant, thus highlighting the importance of incorporating anionic groups into the ligand backbone of WOCs. The beneficial effects of incorporating amide ligand **4** was further illustrated by electrochemical measurements where Ru complex **3** displayed significantly lower redox potentials than WOCs based on both neutral ligand scaffolds and the dicarboxylate ligand of the related [Ru(pdc)(pic)$_3$] complex **10**. Quantum chemical calculations further confirmed the reduced redox potentials associated with Ru complex **3**. This work also highlights the caution that is needed when designing WOCs in the future due to the unforeseen conversion of the envisioned complexes into unexpected metal complexes that are the real catalytic species.

DOI: 10.1021/ic502755c
Inorg. Chem. XXXX, XXX, XXX–XXX

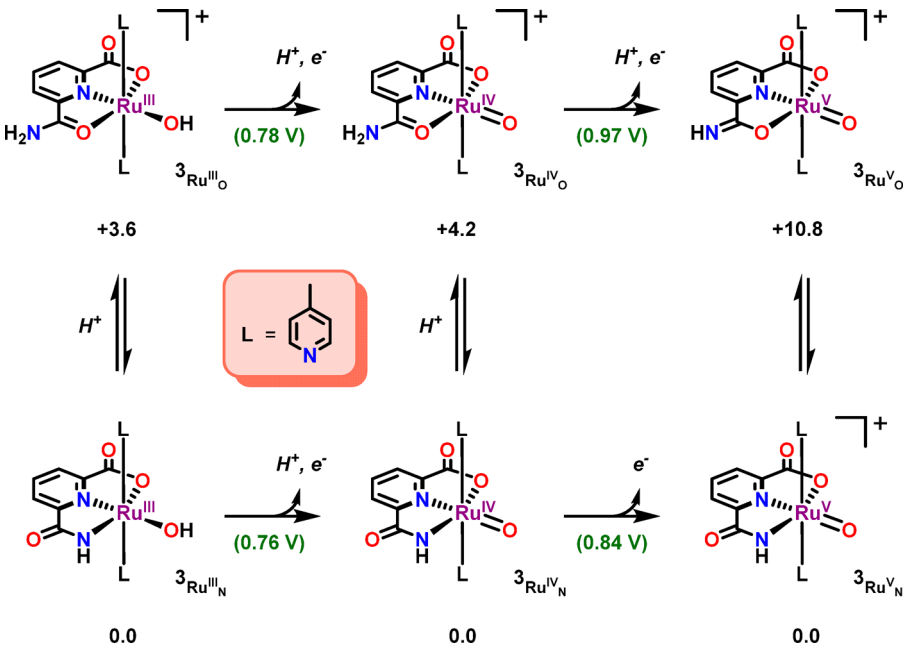

Figure 11. Overview of the various Ru–aqua/hydroxo/oxo intermediates at pH 7.2 with the formal redox states highlighted. Calculated redox potentials are shown in parentheses and are in volts vs normal hydrogen electrode (NHE), and the relative energies for each redox state are given in kcal mol^{-1}.

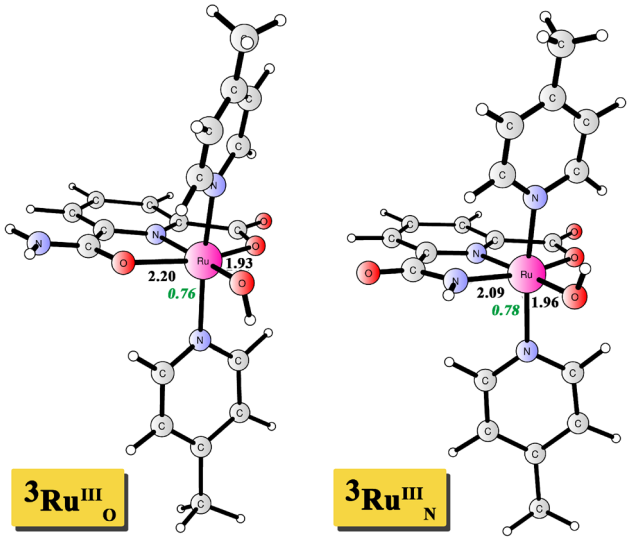

Figure 12. Optimized structures of the two isomers $^{3}Ru^{III}_{O}$ and $^{3}Ru^{III}_{N}$ of Ru complex **3**. Distances are given in angstroms, and the spin densities on Ru are also indicated in italic.

EXPERIMENTAL SECTION

Materials and Methods. ^{1}H NMR spectra were recorded on a 400 or 500 MHz Bruker UltraShield spectrometer (^{13}C NMR spectra at 100 MHz). Chemical shifts (δ) are reported in ppm using residual solvent peak [CD_3OD (δ(H) = 3.31 and (δ(C) = 77.16 ppm); DMSO-d_6 (δ(H) = 2.50 and (δ(C) = 39.52 ppm)] as standard. High-resolution mass spectrometry (HRMS) measurements were recorded on a Bruker Daltonics microTOF spectrometer with an electrospray ionizer. UV–vis absorption spectra were measured on a CARY 300 Bio UV–visible spectrophotometer. Compounds were centrifuged on a Thermo centrifuge CR3i multifunction at 4000 rpm for 15 min.

Single-Crystal X-ray Diffraction. Single-crystal X-ray diffraction data were collected from a red-color needle-like crystal on a SuperNova diffractometer at 100 K using Mo X-ray radiation source (λ = 0.71073 Å) in φ scan mode at Peking University. Data reduction was performed using the CrysAlisPro program,[48] and multiscan adsorption correction was applied. Structure was solved by direct method. Non-hydrogen atoms were located directly from difference Fourier maps. All the hydrogen atoms are located directly in the calculated position based on their geometry. Final structure refinements were performed with the SHELX program[49] by minimizing the sum of the squared deviation of F^2 using a full matrix technique.

Electrochemistry. Electrochemical measurements were carried out with an Autolab potentiostat with a GPES electrochemical interface (Eco Chemie), using a glassy carbon disk (diameter 3 mm) as the working electrode and a platinum spiral as counter electrode. The reference electrode was a saturated calomel electrode (SCE), and the electrolyte used was an aqueous phosphate buffer (0.1 M, pH 7.2). All potentials are reported vs normal hydrogen electrode (NHE), using the $[Ru(bpy)_3]^{3+}/[Ru(bpy)_3]^{2+}$ couple ($E_{1/2}$ = 1.26 V vs NHE) as a reference.

Oxygen Evolution Measurements. A stock solution was made of Ru complex **3** (93 μM) in CH_3CN/H_2O 1:9. The catalyst solutions used in the experiments were then prepared by diluting the stock solution with phosphate buffer (0.1 M, pH 7.2) to the desired concentrations. The resulting solutions were then deoxygenated by bubbling with N_2 for at least 15 min. In a typical run, the chemical oxidant $[Ru(bpy)_3](PF_6)_3$ (3.6 mg, 3.6 μmol) was placed in the reaction chamber and the vessel was evacuated using a TRIVAC pump (model D 2.5E) for 10 min. A pressure of 42 mbar of He was then introduced into the system. After a few minutes the catalyst solution (0.50 mL) was injected into the reaction chamber. The generated oxygen gas was then measured and recorded by MS.

Computational Details. The geometry optimizations in the present study were performed using the density functional B3LYP[50] as implemented in the Gaussian 09 package.[51] The 6-31G(*d*,*p*) basis set was used for the C, N, O, F, H elements and the SDD[52] pseudopotential for Ru. In order to obtain more accurate energies, single-point calculations using these optimized geometries were done employing a larger basis set, where all elements, except Ru, were described by 6-311+G(2*df*,2*p*) at the B3LYP* (15% exact exchange) levels.[53] Solvation effects from the water solvent were calculated using the SMD[54] continuum solvation model with the larger basis set at the B3LYP* levels. Analytic frequency calculations were carried out at the same level of theory as the geometry optimization to obtain the Gibbs free energy corrections and to confirm the nature of the various

DOI: 10.1021/ic502755c
Inorg. Chem. XXXX, XXX, XXX–XXX

Scheme 3. Summary of the Redox Events Proposed to Occur at pH 7.2

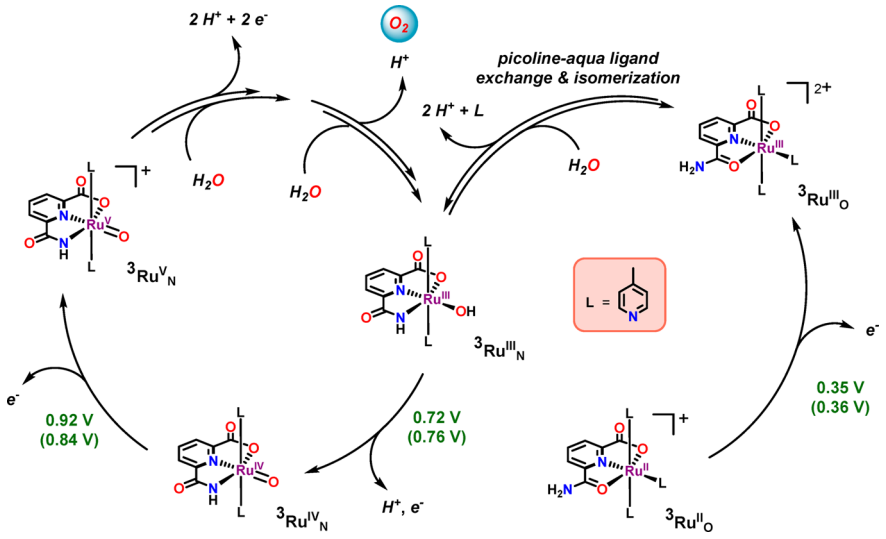

stationary points. Unless otherwise specified, the B3LYP*-D2 energies are reported, including Gibbs free energy corrections from B3LYP and dispersion corrections proposed by Grimme.[55]

To calculate the redox potentials, the absolute redox potential of the $[Ru(bpy)_3]^{3+}/[Ru(bpy)_3)]^{2+}$ couple (1.26 + 4.281 V) was used as the reference,[56] which corresponds to 127.8 kcal mol^{-1} for one-electron oxidation and 407.9 kcal mol^{-1} for proton-coupled one-electron oxidation at pH 7.2. For the latter case, the gas-phase free energy of a proton is −6.3 kcal mol^{-1} and the experimental solvation free energy of a proton (−264.0 kcal mol^{-1}) was used.[57]

Synthesis. $Ru(DMSO)_4Cl_2$[58] and $[Ru(bpy)_3](PF_6)_3$[59] were prepared according to reported procedures. 6-Carbamoylpicolinic acid (**4**, H_3L) and methyl 6-(chlorocarbonyl)picolinate (**8**) were synthesized according to previously reported procedures.[60] 2,6-Pyridinedicarboxylic acid, hydrazine hydrate (Sigma-Aldrich) and methanol (VWR, HPLC grade) were used as received without further purification.

6-Carbamoylpicolinic Acid (4, H_3L). ^{1}H NMR (400 MHz, DMSO-d_6): δ = 8.31 (s, 1H), 7.88−8.04 (m, 3H), 7.71 (s, 1H). ^{13}C NMR (100 MHz, DMSO-d_6): δ = 167.80, 166.51, 55.76, 149.09, 137.67, 125.95, 121.87. HRMS-ESI: calcd for $C_{16}H_{14}N_4O_6$ $[M + Na^+]^+$, 189.0271; found, 189.0267.

Synthesis of Dimethyl 6,6′-(Hydrazine-1,2-dicarbonyl)-dipicolinate (9). Compound **9** was prepared by dissolving compound **8** (1.00 g, 5.52 mmol) in dry CH_2Cl_2 (20 mL) followed by addition of $N_2H_4{\cdot}H_2O$ (120 μL, 2.50 mmol) and Et_3N (4.60 mL, 33.1 mmol). The mixture was then stirred at room temperature for 12 h. Aqueous saturated Na_2HCO_3 solution (50 mL) was then added and the mixture was extracted with CH_2Cl_2 (3 × 20 mL). The organic layer was washed with 1 M HCl (2 × 20 mL) and dried over anhydrous Na_2SO_4. Removal of the solvent in vacuo yielded the pure product as a white solid (0.760 g, 40%). ^{1}H NMR (400 MHz, $CDCl_3$): δ = 10.26 (s, 2H), 8.39 (dd, J = 7.6, 0.8 Hz, 2H), 8.29 (dd, J = 8.0, 1.2 Hz, 2H), 8.05 (t, J = 8.0 Hz, 2H), 4.03 (s, 6H). ^{13}C NMR (100 MHz, $CDCl_3$): δ = 164.96, 160.92, 148.61, 147.17, 138.82, 128.09, 125.82, 53.13. HRMS-ESI: calcd for $C_{16}H_{14}N_4O_6$ $[M + Na^+]^+$, 381.0806; found, 381.0819.

Synthesis of 6,6′-(Hydrazine-1,2-dicarbonyl)dipicolinic Acid (1). Compound **9** (0.100g, 0.28 mmol) was dissolved in THF/H_2O (3:2, 5 mL), and LiOH (0.016g, 0.70 mmol) was added. The mixture was refluxed for 4 h and acidified with 1 M HCl. The formed precipitate was filtered to give the title compound as a white solid (0.086 g, 93%). ^{1}H NMR (400 MHz, DMSO-d_6): δ = 11.29 (brs, 2H), 8.35−8.27 (m, 6H). ^{13}C NMR (100 MHz, DMSO-d_6): δ = 164.67, 162.14, 148.05, 146.26, 140.28, 127.22, 125.84. HRMS-ESI: calcd for $C_{16}H_{14}N_4O_6$ $[M + Na^+]^+$, 353.0493; found, 353.0485.

Synthesis of Ru Complex 3 from Ligand 1. To a mixture of 6,6′-(hydrazine-1,2-dicarbonyl)dipicolinic acid (**1**, 0.050 g, 0.15 mmol) and Et_3N (0.20 mL, 1.5 mmol) in MeOH (5.0 mL) was added $Ru(DMSO)_4Cl_2$ (0.16 g, 0.33 mmol). The solution was degassed with N_2 and refluxed overnight. After 16 h, an excess of 4-picoline (0.40 mL, 4.5 mmol) was added and the resulting solution was further refluxed for another 48 h. The reaction mixture was then cooled to room temperature and NH_4PF_6 (0.099 g, 0.61 mmol) was added, and the resulting solution was stirred for another 30 min at room temperature. To the mixture was added deionized H_2O (15 mL). The resulting suspension was centrifuged and the precipitate was discarded. The supernatant was concentrated in vacuo, and EtOAc/CH_3CN (4:1, 2.0 mL) was added then the mixture was left to stand at room temperature for a couple of hours. The precipitate which formed was centrifuged to give Ru complex **3** ($[Ru(HL)(pic)_3](PF_6)$) as red crystals (0.060 g, 29%).

Synthesis of Ru Complex 3 from Ligand 4. To a mixture of 6-carbamoylpyridine-2-carboxylic acid (**4**, 0.057 g, 0.35 mmol) and Et_3N (0.50 mL, 3.5 mmol) in MeOH (10 mL) was added $Ru(DMSO)_4Cl_2$ (0.17 g, 0.35 mmol). The solution was degassed with N_2 and refluxed overnight. After 16 h, an excess of 4-picoline (1.0 mL, 10.5 mmol) was added, and the resulting solution was further refluxed for another 48 h. The reaction mixture was then cooled to room temperature and NH_4PF_6 (0.17 g, 1.05 mmol) was added, and the resulting solution was stirred for another 30 min at room temperature. To the mixture was added deionized H_2O (15 mL). The resulting suspension was centrifuged and the precipitate was discarded. The supernatant was concentrated in vacuo, and EtOAc/CH_3CN (4:1, 2.0 mL) was added then the mixture was left to stand at room temperature for a couple of hours. The precipitate which formed was centrifuged to give Ru complex **3** (isolated as a mixture of the PF_6^- and Cl^- salt, $[Ru(HL)(pic)_3](PF_6)_{0.5}Cl_{0.5}$) as red crystals (0.12 g, 50%). ^{1}H NMR (500 MHz, CD_3OD in the presence of ascorbic acid): δ = 8.64−8.63 (m, 2H), 8.36 (dd. J = 8.00, 1.00 Hz, 1H), 8.09 (dd, J = 8.00, 1.00 Hz, 1H), 7.86 (t, J = 8.00 Hz, 1H), 7.84−7.82 (m, 4H), 7.80 (s, 1H), 7.33−7.31 (m, 2H), 7.10−7.09 (m, 4H), 2.44 (s, 3H), 2.29 (s, 6H). HRMS-ESI: calcd for $C_{25}H_{25}N_5O_3Ru$ $[M - PF_6^-]^+$, 545.1002; found, 545.1006. Anal. Calcd (%) for $C_{28}H_{30.5}Cl_{0.5}F_3N_{5.5}O_4P_{0.5}Ru$ ($[Ru(HL)(pic)_3](PF_6)_{0.5}Cl_{0.5}{\cdot}0.5EtOAc{\cdot}0.5CH_3CN$): C, 48.09%; H, 4.40%; N, 11.02%. Found: C, 48.03%; H, 4.54%; N, 10.82%.

■ ASSOCIATED CONTENT

Supporting Information

^{1}H NMR, ^{13}C NMR, high-resolution mass spectrometry, UV−vis spectra, and X-ray crystallographic data. The Supporting Information is available free of charge on the ACS Publications website at DOI: 10.1021/ic502755c.

DOI: 10.1021/ic502755c
Inorg. Chem. XXXX, XXX, XXX−XXX

AUTHOR INFORMATION

Corresponding Authors

*E-mail: markusk@organ.su.se.
*E-mail: phera@organ.su.se.
*E-mail: bjorn.akermark@organ.su.se.

Notes

The authors declare no competing financial interest.

ACKNOWLEDGMENTS

Financial support from the Swedish Research Council (621-2013-4872 and 348-2014-6070), the Knut and Alice Wallenberg Foundation, and the Carl Trygger Foundation is gratefully acknowledged.

REFERENCES

(1) Kärkäs, M. D.; Johnston, E. V.; Verho, O.; Åkermark, B. *Acc. Chem. Res.* **2014**, *47*, 100−111.
(2) Armaroli, N.; Balzani, V. *Angew. Chem., Int. Ed.* **2007**, *46*, 52−66.
(3) Nocera, D. G. *ChemSusChem* **2009**, *2*, 387−390.
(4) Umena, Y.; Kawakami, K.; Shen, J.-R.; Kamiya, N. *Nature* **2011**, *473*, 55−60.
(5) Kärkäs, M. D.; Verho, O.; Johnston, E. V.; Åkermark, B. *Chem. Rev.* **2014**, *114*, 11863−12001.
(6) Karlsson, E. A.; Lee, B.-L.; Åkermark, T.; Johnston, E. V.; Kärkäs, M. D.; Sun, J.; Hansson, Ö.; Bäckvall, J.-E.; Åkermark, B. *Angew. Chem., Int. Ed.* **2011**, *50*, 11715−11718.
(7) Young, K. J.; Takase, M. K.; Brudvig, G. W. *Inorg. Chem.* **2013**, *52*, 7615−7622.
(8) Karlsson, E. A.; Lee, B.-L.; Liao, R.-Z.; Åkermark, T.; Kärkäs, M. D.; Saavedra Becerril, V.; Siegbahn, P. E. M.; Zou, X.; Abrahamsson, M.; Åkermark, B. *ChemPlusChem* **2014**, *79*, 936−950.
(9) Arafa, W. A. A.; Kärkäs, M. D.; Lee, B.-L.; Åkermark, T.; Liao, R.-Z.; Berends, H.-M.; Messinger, J.; Siegbahn, P. E. M.; Åkermark, B. *Phys. Chem. Chem. Phys.* **2014**, *16*, 11950−11964.
(10) Liao, R.-Z.; Kärkäs, M. D.; Lee, B.-L.; Åkermark, B.; Siegbahn, Per E. M. *Inorg. Chem.* **2015**, *54*, 342−351.
(11) Acuña-Parés, F.; Codolà, Z.; Costas, M.; Luis, J. M.; Lloret-Fillol, J. *Chem.—Eur. J.* **2014**, *20*, 5696−5707.
(12) Ellis, W. C.; McDaniel, N. D.; Bernhard, S.; Collins, T. J. *J. Am. Chem. Soc.* **2010**, *132*, 10990−10991.
(13) Liao, R.-Z.; Li, X.-C.; Siegbahn, P. E. M. *Eur. J. Inorg. Chem.* **2014**, 728−741.
(14) Parent, A. R.; Nakazono, T.; Lin, S.; Utsunomiya, S.; Sakai, K. *Dalton Trans.* **2014**, *43*, 12501−12513.
(15) Wang, D.; Groves, J. T. *Proc. Natl. Acad. Sci. U. S. A.* **2013**, *110*, 15579−15584.
(16) Lv, H.; Song, J.; Geletii, Y. V.; Vickers, J. W.; Sumliner, J. M.; Musaev, D. G.; Kögerler, P.; Zhuk, P. F.; Bacsa, J.; Zhu, G.; Hill, C. L. *J. Am. Chem. Soc.* **2014**, *136*, 9268−9271.
(17) Zhou, X.; Li, F.; Li, H.; Zhang, B.; Yu, F.; Sun, L. *ChemSusChem* **2014**, *7*, 2453−2456.
(18) Zhang, M.-T.; Chen, Z.; Kang, P.; Meyer, T. J. *J. Am. Chem. Soc.* **2013**, *135*, 2048−2051.
(19) Winikoff, S. G.; Cramer, C. J. *Catal. Sci. Technol.* **2014**, *4*, 2484−2489.
(20) Zhang, T.; Wang, C.; Liu, S.; Wang, J.-L.; Lin, W. *J. Am. Chem. Soc.* **2014**, *136*, 273−281.
(21) Diaz-Morales, O.; Hersbach, T. J. P.; Hetterscheid, D. G. H.; Reek, J. N. H.; Koper, M. T. M. *J. Am. Chem. Soc.* **2014**, *136*, 10432−10439.
(22) Parent, A. R.; Brewster, T. P.; De Wolf, W.; Crabtree, R. H.; Brudvig, G. W. *Inorg. Chem.* **2012**, *51*, 6147−6152.
(23) Hintermair, U.; Hashmi, S. M.; Elimelech, M.; Crabtree, R. H. *J. Am. Chem. Soc.* **2012**, *134*, 9785−9795.
(24) Kärkäs, M. D.; Åkermark, T.; Chen, H.; Sun, J.; Åkermark, B. *Angew. Chem., Int. Ed.* **2013**, *52*, 4189−4193.
(25) Zhang, G.; Chen, K.; Chen, H.; Yao, J.; Shaik, S. *Inorg. Chem.* **2013**, *52*, 5088−5096.
(26) Muckerman, J. T.; Kowalczyk, M.; Badiei, Y. M.; Polyansky, D. E.; Concepcion, J. J.; Zong, R.; Thummel, R. P.; Fujita, E. *Inorg. Chem.* **2014**, *53*, 6904−6913.
(27) Li, T.-T.; Chen, Y.; Li, F.-M.; Zhao, W.-L.; Wang, C.-J.; Lv, X.-J.; Xu, Q.-Q.; Fu, W.-F. *Chem.—Eur. J.* **2014**, *20*, 8054−8061.
(28) Wang, Y.; Ahlquist, M. S. G. *Phys. Chem. Chem. Phys.* **2014**, *16*, 11182−11185.
(29) Tamaki, Y.; Vannucci, A. K.; Dares, C. J.; Binstead, R. A.; Meyer, T. J. *J. Am. Chem. Soc.* **2014**, *136*, 6854−6857.
(30) Isobe, H.; Tanaka, K.; Shen, J.-R.; Yamaguchi, K. *Inorg. Chem.* **2014**, *53*, 3973−3984.
(31) Neudeck, S.; Maji, S.; López, I.; Meyer, S.; Meyer, F.; Llobet, A. *J. Am. Chem. Soc.* **2014**, *136*, 24−27.
(32) Badiei, Y. M.; Polyansky, D. E.; Muckerman, J. T.; Szalda, D. J.; Haberdar, R.; Zong, R.; Thummel, R. P.; Fujita, E. *Inorg. Chem.* **2013**, *52*, 8845−8850.
(33) Duan, L.; Moyses, C. A.; Ahlquist, M. S. G.; Sun, L. *Proc. Natl. Acad. Sci. U. S. A.* **2012**, *109*, 15584−15588.
(34) Kang, R.; Chen, K.; Yao, J.; Shaik, S.; Chen, H. *Inorg. Chem.* **2014**, *53*, 7130−7136.
(35) Laine, T. M.; Kärkäs, M. D.; Liao, R.-Z.; Åkermark, T.; Lee, B.-L.; Karlsson, E. A.; Siegbahn, P. E. M.; Åkermark, B. *Chem. Commun.* **2015**, *51*, 1862−1865.
(36) Kärkäs, M. D.; Åkermark, T.; Johnston, E. V.; Karim, S. R.; Laine, T. M.; Lee, B.-L.; Åkermark, T.; Privalov, T.; Åkermark, B. *Angew. Chem., Int. Ed.* **2012**, *51*, 11589−11593.
(37) Xu, Y.; Åkermark, T.; Gyollai, V.; Zou, D.; Eriksson, L.; Duan, L.; Zhang, R.; Åkermark, B.; Sun, L. *Inorg. Chem.* **2009**, *48*, 2717−2719.
(38) Kärkäs, M. D.; Johnston, E. V.; Karlsson, E. A.; Lee, B.-L.; Åkermark, T.; Shariatgorji, M.; Ilag, L.; Hansson, Ö.; Bäckvall, J.-E.; Åkermark, B. *Chem.—Eur. J.* **2011**, *17*, 7953−7959.
(39) Xu, Y.; Fischer, A.; Duan, L.; Tong, L.; Gabrielsson, E.; Åkermark, B.; Sun, L. *Angew. Chem., Int. Ed.* **2010**, *49*, 8934−8937.
(40) Lee, B.-L.; Kärkäs, M. D.; Johnston, E. V.; Inge, A. K.; Tran, L.-H.; Xu, Y.; Hansson, Ö.; Zou, X.; Åkermark, B. *Eur. J. Inorg. Chem.* **2010**, 5462−5470.
(41) Norrby, T.; Börje, A.; Åkermark, B.; Hammarström, L.; Alsins, J.; Lashgari, K.; Norrestam, R.; Mårtensson, J.; Stenhagen, G. *Inorg. Chem.* **1997**, *36*, 5850−5858.
(42) Duan, L.; Xu, Y.; Gorlov, M.; Tong, L.; Andersson, S.; Sun, L. *Chem.—Eur. J.* **2010**, *16*, 4659−4668.
(43) Nyhlen, J.; Duan, L.; Åkermark, B.; Sun, L.; Privalov, T. *Angew. Chem., Int. Ed.* **2010**, *49*, 1773−1777.
(44) For further information on how to calculate the turnover frequency (TOF), see Supporting Information.
(45) Migliore, A.; Polizzi, N. F.; Therien, M. J.; Beratan, D. N. *Chem. Rev.* **2014**, *114*, 3381−3465.
(46) Wenger, O. S. *Coord. Chem. Rev.* **2015**, *282*−*283*, 150−158.
(47) Tong, L.; Wang, Y.; Duan, L.; Xu, Y.; Cheng, X.; Fischer, A.; Ahlquist, M. S. G.; Sun, L. *Inorg. Chem.* **2012**, *51*, 3388−3398.
(48) *CrysAlis Software System*, version 171.37.33; Agilent Technologies: Santa Clara, CA, 2014.
(49) (a) Sheldrick, G. M. *Acta Crystallogr., Sect. A: Found. Crystallogr.* **2008**, *64*, 112−122. (b) Sheldrick, G. M. *SHELXS97, Program for Solution of Crystal Structure*; University of Gottingen: Gottingen, Germany, 1997.
(50) Becke, A. D. *J. Chem. Phys.* **1993**, *98*, 5648−5652.
(51) Frisch, M. J.; Trucks, G. W.; Schlegel, H. B.; Scuseria, G. E.; Robb, M. A.; Cheeseman, J. R.; Scalmani, G.; Barone, V.; Mennucci, B.; Petersson, G. A.; Nakatsuji, H.; Caricato, M.; Li, X.; Hratchian, H. P.; Izmaylov, A. F.; Bloino, J.; Zheng, G.; Sonnenberg, J. L.; Hada, M.; Ehara, M.; Toyota, K.; Fukuda, R.; Hasegawa, J.; Ishida, M.; Nakajima, T.; Honda, Y.; Kitao, O.; Nakai, H.; Vreven, T.; Montgomery, J. A., Jr.; Peralta, J. E.; Ogliaro, F.; Bearpark, M.; Heyd, J. J.; Brothers, E.; Kudin, K. N.; Staroverov, V. N.; Kobayashi, R.; Normand, J.; Raghavachari, K.; Rendell, A.; Burant, J. C.; Iyengar, S. S.; Tomasi, J.; Cossi, M.; Rega,

DOI: 10.1021/ic502755c
Inorg. Chem. XXXX, XXX, XXX−XXX

N.; Millam, J. M.; Klene, M.; Knox, J. E.; Cross, J. B.; Bakken, V.; Adamo, C.; Jaramillo, J.; Gomperts, R.; Stratmann, R. E.; Yazyev, O.; Austin, A. J.; Cammi, R.; Pomelli, C.; Ochterski, J. W.; Martin, R. L.; Morokuma, K.; Zakrzewski, V. G.; Voth, G. A.; Salvador, P.; Dannenberg, J. J.; Dapprich, S.; Daniels, A. D.; Farkas, Ö.; Foresman, J. B.; Ortiz, J. V.; Cioslowski, J.; Fox, D. J. *Gaussian 09*, revision B.01; Gaussian, Inc.; Wallingford, CT, 2009.
(52) Andrae, D.; Häussermann, U.; Dolg, M.; Stoll, H.; Preuss, H. *Theor. Chim. Acta* **1990**, *77*, 123−141.
(53) Reiher, M.; Salomon, O.; Hess, B. A. *Theor. Chem. Acc.* **2001**, *107*, 48−55.
(54) Marenich, A. V.; Cramer, C. J.; Truhlar, D. G. *J. Phys. Chem. B* **2009**, *113*, 6378−6396.
(55) Grimme, S. *J. Comput. Chem.* **2006**, *27*, 1787−1799.
(56) Isse, A. A.; Gennaro, A. *J. Phys. Chem. B* **2010**, *114*, 7894−7899.
(57) Camaioni, D. M.; Schwerdtfeger, C. A. *J. Phys. Chem. A* **2005**, *109*, 10795−10797.
(58) Dulière, E.; Devillers, M.; Marchand-Brynaert, J. *Organometallics* **2003**, *22*, 804−811.
(59) DeSimone, R. E.; Drago, R. S. *J. Am. Chem. Soc.* **1970**, *92*, 2343−2352.
(60) (a) Ong, W. Q.; Zhao, H.; Fang, X.; Woen, S.; Zhou, F.; Yap, W.; Su, H.; Li, S. F. Y.; Zeng, H. *Org. Lett.* **2011**, *13*, 3194−3197. (b) Tondreau, A. M.; Darmon, J. M.; Wile, B. M.; Floyd, S. K.; Lobkovsky, E.; Chirik, P. J. *Organometallics* **2009**, *28*, 3928−3940. (c) Yang, Z.; Tang, R.; Zhang, Z. *J. Mol. Struct.* **2012**, *1030*, 19−25.

DOI: 10.1021/ic502755c
Inorg. Chem. XXXX, XXX, XXX−XXX